Thermal behavior of cold plate storage cask for used Light Water Reactor nuclear fuels

A Thesis
Presented in Partial Fulfillment of the Requirements for the
Degree of Master of Science
with a
Major in Nuclear Engineering
in the
College of Graduate Studies
University of Idaho
by
Winfred A. K. Sowah

Major Professor: Richard Christensen, Ph.D.
Committee Members: Robert Borrelli, Ph.D.; David Arcilesi, Ph.D.; Haiyan Zhao, Ph.D.
Department Administrator: Richard Christensen, Ph.D.

December 2019

AUTHORIZATION TO SUBMIT THESIS

This thesis of Winfred A. K. Sowah, submitted for the degree of Master of Science with a Major in Nuclear Engineering and titled "Thermal behavior of cold plate storage cask for used Light Water Reactor nuclear fuels," has been reviewed in final form. Permission, as indicated by the signatures and dates below, is now granted to submit final copies to the College of Graduate Studies for approval.

Major Professor: _____ Date: _____
Richard Christensen, Ph.D.

Committee Members: _____ Date: _____
Robert Borrelli, Ph.D.

_____ Date: _____
David Arcilesi, Ph.D.

_____ Date: _____
Haiyan Zhao, Ph.D.

Department Administrator: _____ Date: _____
Richard Christensen, Ph.D.

ABSTRACT

An experimental and analytical study is reported for the thermal behavior of a cold plate storage cask. The cold plates are designed to actively cool UO_2 used fuel bundles from pressurized water reactors (PWRs) and boiling water reactors (BWRs) and are manufactured based on a proprietary pipe-casting technology by Sakae Casting LLC.

For the experiment, four cold plates corresponding to approximately a one-third scale height of a 17x17 PWR fuel bundle assembly were constructed into a cask. The cask was thermally tested using electric heaters at temperatures ranging from 100 ^{o}C to 600 ^{o}C. This resulted in evaluated heat transfer coefficients at the cask inner walls ranging from 4.01 to 6.92 W/m^{2}K.

An analytical study was also performed for a 1 to 7-year old used fuel at discharge a burnup of 50 GWd/MTHM to evaluate the expected heat transfer coefficients on the inner walls of the cold plate cask as a function of the decay heat of the fuel. A full size 17x17 PWR fuel bundle assembly and its corresponding cold plate cask geometry is used for the study. A homogenous distribution of heat flux within the bundle was assumed, and the calculated heat transfer coefficients in the cask ranged from 8.08 to 7.72 W/m^{2}K at the heater surface and from 4 to 3.45 W/m^{2}K at the slab surface.

ACKNOWLEDGEMENTS

My sincere appreciation goes to my committee members. Dr. Richard Christensen has been a great mentor and advisor through every step of this project. I am grateful to him for offering his wealth of knowledge and depth of experience as resources for completing this thesis. I thank Dr. David Arcilesi for his time, expertise and patience. I thank Dr. Robert Borelli and Dr. Haiyan Zhao for the breadth and depth of experience they brought to the committee.

I would also like to thank Larry Zirker for his endless patience, knowledge, and mentorship throughout this project. I also thank Jesse Webb, Joseph Hafen, Amey Shigrekar, and Eugene Engmann for their invaluable assistance.

DEDICATION

Most importantly, I would like to thank my parents, William and Joselyn Sowah, for their immeasurable sacrifices to provide me a quality education and the most loving home in which to grow up. I am ever grateful for the love and encouragement of my siblings Calvin and Reginald Sowah. Lastly, I thank my dear companion, joy and love of my life, Esitia Sowah for her support and understanding that helped in completing this thesis.

TABLE OF CONTENTS

List of Tables

List of Figures

CHAPTER 1: Introduction

With the current fleet of operating nuclear reactors, the quantities of used fuel is continually increasing. Current estimates in metric tons of heavy metal of used fuel are 10900 in the Republic of Korea, 19000 in Japan, 13500 in France and 69000 in the USA [1]. While France reprocesses or recycles used fuel after the cooling period, Japan and the Republic of Korea have plans to also reprocess their used fuel [2]. The USA does not reprocess used nuclear fuel [3]. The policy regarding this waste is direct disposal into a deep geological repository. Yet, used fuel requires a cooling period for either reprocessing or permanent storage.

The USA has 99 commercial power plants generating about 805 TWh of electricity per year making it the world's largest producer of nuclear power. As of 2015, the USA has almost 100 pools nearly filled with used fuel. Used fuel is therefore moved into dry casks to save space. Along with the political sensitivity of building additional storage pools is the disadvantage of the substantial amount of space and water required by the current pool cooling system. Safety and security measures require that pools are located indoors and that water levels are monitored to ensure ready water supply for a possible emergency.

This study presents an alternative to the currently used fuel cooling system and analyzes the thermal behavior of a cask constructed with 'Cold Plate' technology using aluminum material.The Cold Plate is a water-cooled, thin cooling plate that is combined with proprietary casting methods by Sakae Casting Co., LTD.

The cold plate has been adopted for high performance of semiconductor equipment by direct contact with the coolant [4]. The design maintains low temperature and allows for a significant decrease in temperature for the integrated circuit chips and diodes. With this design, the energy consumption and space requirements are much smaller than current air-cooled systems. The cold plate is used in various fields including battery trays for electric vehicles and water production line equipment.

Sakae has developed a prototype that is compact, efficient and prone to very minimal failure. The vision for this technology is to improve the safety of fuel management by reducing and preventing further accidents with this cooling device while potentially lowering maintenance costs.

CHAPTER 2: Background and literature review

UO_2 fuel in PWRs are replaced about every 18 months because the enrichment level for commercial reactors of 5% has reduced to less than 1%. Additionally, fission products form in the fuel as by-products which strongly absorb neutrons and greatly inhibit fission. The removed fuel is highly radioactive and emits significant amounts of heat. This fuel is stored in large pools in the power plant that are about 40 feet deep for 10 to 20 years to allow radioactive decay to occur and the heat load to lessen. The water provides radiation shielding for occupational safety and cooling of the fuel via pumps that circulate the water for constant heat removal. The fuel is strategically placed in pools to maintain subcriticality.

After a cooling period, the used fuel is placed in a dry cask for storage outside the facility. Although these casks are robust, only about 31 % of the used fuel is stored in them with the remaining 69 % stored in used fuel pools. Cooling pools can lose water in an accident and the fuel can melt and possible release radioactive materials.

Interim storage of spent Light Water Reactor (LWR) fuel is a pertinent matter of consideration in many countries. Owing to the estimated accumulation of spent fuel in relation to proposed agendas for permanent handling of LWR fuel, interim storage in power plant pools and additional away-from-reactor facilities play a crucial role in spent fuel management [5].

Interim storage measures for fuel assemblies may extend over decades. Therefore, research and development efforts have been undertaken to examine the integrity of spent fuel assemblies and their handling capability throughout the anticipated storage periods and during shipment to more permanent locations or for reprocessing where applicable.

2.1 Wet Storage

Fuel assemblies are stored under deionized water at temperatures below 40 ^{o}C [6]. In a study by Peehs et al [7], of the behavior of used LWR fuels, it was observed that there is no additional corrosion of zircaloy cladding tubes under these conditions. Also, at 40 ^{o}C, the micro- and macro distributions of hydrogen and zirconium hydride particles are stable and that the stresses resulting from well-controlled manipulation of LWR spent fuel do not cause any problems. Finally, stresses caused by inner pressure in spent fuel rods do not affect integrity since they only amount to about

10% of the yield point [6], [7]. A summary of mechanisms potentially degrading the integrity of the fuel cladding is shown in Figure 2.1.

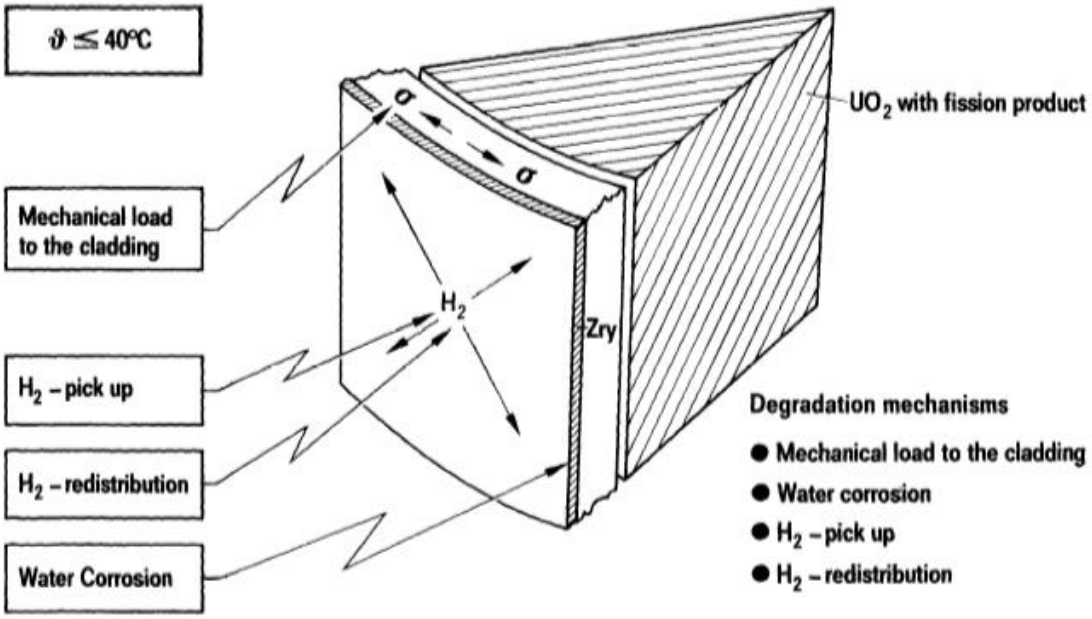

Figure 2.1: Mechanisms affecting spent fuel cladding performance during wet storage [7]

2.2 Dry Storage

Fuel is stored in shielded containers outside the reactor containment buildings and has the advantage of offering flexibility in system types that can be tailored to the needs of a specific site, while providing long-term storage with low maintenance and ready expandability [8]. Storage casks become even more attractive to utilities if they are equipped for use as shipping containers hence eliminating the need to put the fuel back into the reactor fuel transfer pool to transfer it to a shipping container [8]. Consequently, plant owners can avoid potential mishaps in handling spent fuel that could result in a reportable incident that would affect the record of the entire nuclear industry [8].

Figure 2.2 shows a compilation of all noteworthy potential degradation mechanisms [7]. Kasper et al in their study of used fuel behavior observed that oxidation resulting from impurities of

technical grade inert gases used as storage media may be neglected and that the same holds true for hydrogen pick-up from the residual moisture and hydrogen redistribution due to thermal diffusion [9]. Also, fuel rod thermal fission may be excluded since no further fission products are released during extended storage and crack propagation does not occur in the case of crack sizes smaller than 300 μm and temperatures less than 450 ^{o}C [9].

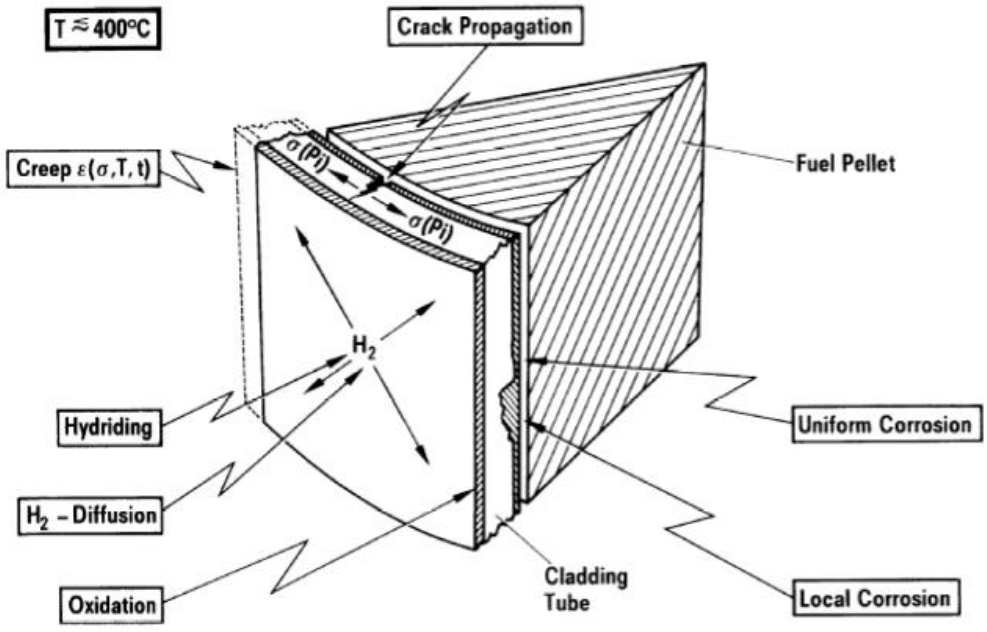

Figure 2.2: Mechanisms affecting spent fuel cladding performance during dry storage [7]

Peehs et al [11] undertook instrumented experiments with complete PWR fuel bundles to improve the database of dry storage of spent LWR fuel. The bundles used were composed of rods of different design and burnup to an average rod burnup of more than 40 GWd/tU accumulated during four reactor cycles [9],[12]. The experiments were performed in a specially designed dry storage box (Figure 2.3). Each bundle was instrumented with 13 thermocouples to continuously measure the cladding temperature. Gas samples were taken from the storage box to investigate the fuel rod integrity.

The first experiment was performed with a fuel assembly after a 10-month decay time, generating about 2 kW of decay heat. The maximum assembly temperature recorded was 300 ^{o}C. This temperature decreased to 270 ^{o}C after 60 days when the test was terminated. The gas samples taken indicated that the fuel rods were fully intact.

The second experiment used a fuel assembly with 4.5 months of decay time, generating about 3 kW of decay heat. The maximum assembly temperature reached 400 ºC (Figure 2.4). There was no indication of any defect throughout the total test. Careful post-pile inspection did not indicate any change in the fuel assembly in agreement with the theoretical assessment.

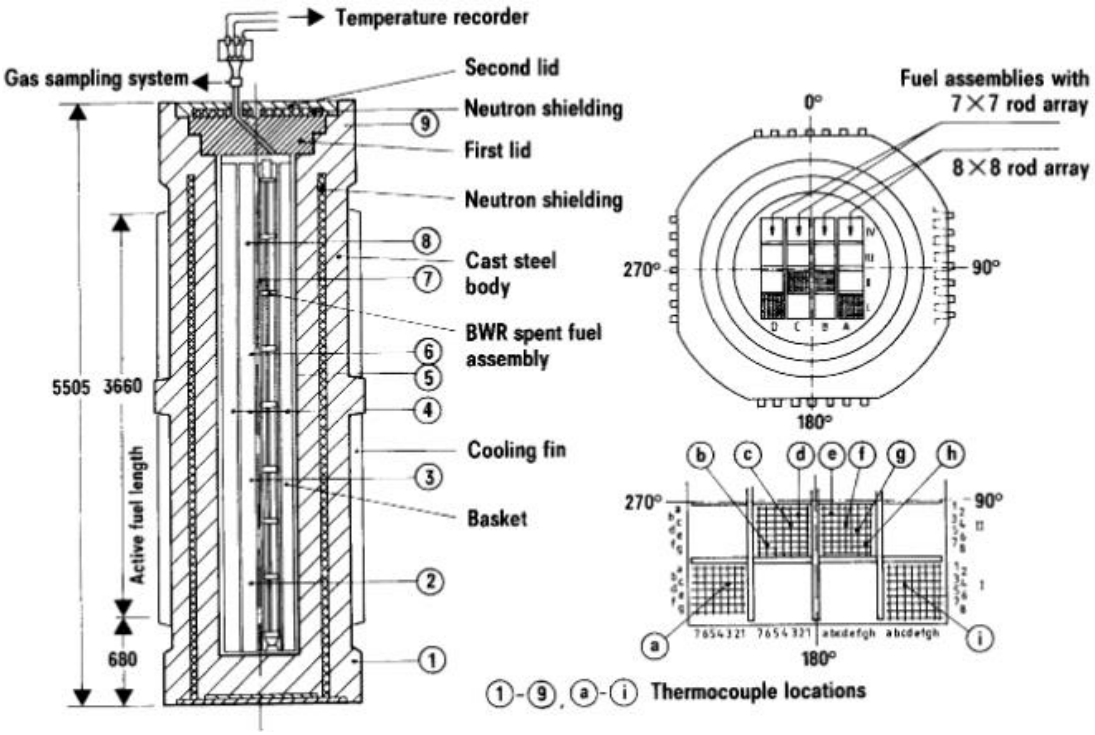

Figure 2.3: Schematic of BWR used fuel assembly thermocouple positions [7]

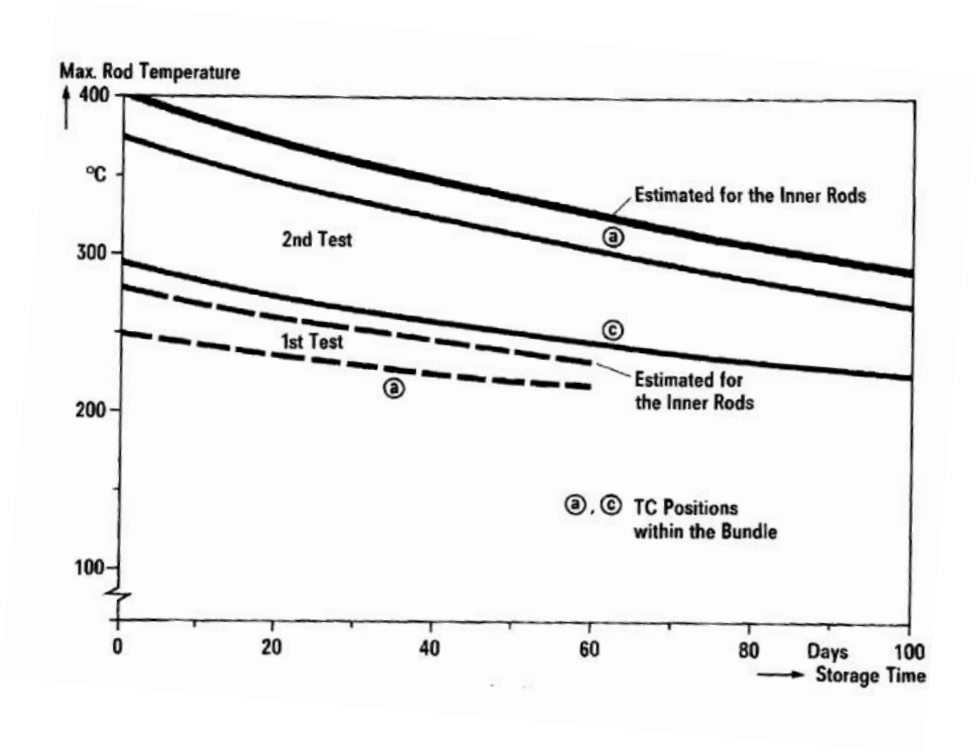

Figure 2.4: Temperature history of dry storage tests during first 100 days of storage by Peehs el al [10].

In summarizing their findings on spent fuel behavior in relation to present-day interim storage concepts, Peehs et al concluded that dry storage under inert gases are not expected to cause any cladding failures over the interim storage period as long as the dry storage temperature is limited to 450 ^{o}C [11].

2.3 Temperature profiles of dry cask storage systems

In a gap analysis by the DOE to support extended storage of spent nuclear fuels [13], temperature profiles of dry casks were selected as the high-priority, cross-cutting area in need of research and development. This majorly stems from the fact that most degradation mechanisms are temperature-dependent, with rates generally increasing as temperature rises. Safety analyses currently in place are appropriately based on bounding temperature profiles but recent data showed that high-burnup cladding alloys can become brittle at lower temperatures owing to phenomena like

radial hydride reorientation [14]. For these reasons, there is a recognizable need to obtaining realistic, temperature estimates for dry storage components over time. Table 2.1 summarizes the dry cask storage systems commonly in use in the U.S. The two general types of storage systems include, (1) self-contained shielded metallic casks without an overpack and (2) metallic canisters with a separate overpack to provide radiation shielding and physical protection.

Table 2.1: Summary of dry cask storage systems in common use in the U.S.[15]

Vendor	System	Cask/Canister	Type*	Closure
Energy Solutions	FuelSolutions	VSC-24, W150	C/O	Welded
General Nuclear Systems, Inc.	CASTOR	V/21, X/33	Cask	Bolted
Holtec International	HI-STAR-100	MPC-68, MPC-80	C/O	Welded
	HI-STORM-100	MPC-24, MPC-32, MPC-68	C/O	Welded
NAC International, Inc.	S/T	NAC-I28	Cask	Bolted
	MPC	MPC-26, MPC-36	C/O	Welded
	UMS	UMS-24	C/O	Welded
	MAGNASTOR	MAGNASTOR	C/O	Welded
Transnuclear, Inc.	NUHOMS	52B, 61BT, 61BTH, 7P, 24P, 24PHB, 24PT, 24PTH, 24PT1, 32P, 32PT, 32PTH, 12T, HD	C/O	Welded
	TN Metal Casks	TN-24, TN-32, TN-40, TN-68	Cask	Bolted
Westinghouse	MC-10	MC-10	Cask	Bolted

Cask = self-contained metallic cask without overpack.
* C/O = metallic canister with overpack.

Most thermal analyses of used fuel storage casks have primarily been done for certification purposes. They include detailed component geometries, analytical methods and results in compliance with corresponding regulations as specified in the US 10 CFR 72. The thermal analyses are usually outlined in Chapter 4 of the safety analysis reports obtained from the NRC's library [16]. It is due to such certification purposes that thermal performance has been typically analyzed in a conservative way to create enough temperature margin for thermal safety.

There are reported studies on natural convection of heat transfer in a closed canister. Earlier work pertaining to this area has been reviewed by Xie et al [17]. Nishimura et al [18] undertook an experimental and numeric study of natural convection in a horizontal storage cask housing 24 electrically heated dummy fuel assemblies that used water or air as the cooling medium. The experimental cask scaled at one fifth (1/5) of an actual dry shielded canister generated Rayleigh numbers varying from $3x10^7$ to $2x10^8$, based on the inner radius of the canister. The overall heat transfer coefficients were found to be proportional to the one fourth (1/4) power of the Rayleigh (Ra)

number, while the sleeve surface temperatures calculated using a 2D model agreed with the experimental data within 8%.

Later analyses by Xie et al [17] and more recently by Lee et al [19] to verify their 2-D computer simulations of horizontal storage casks used the commercial codes of PHOENICS-3.2 and FLUENT 13.5 respectively. The simulation by Xie et al [17] was on the same topic as Nishimura et al [18], however, it included both laminar and turbulent models with Ra number up to 10^9. The computational results for the laminar model agreed with Nishimura's experiment but the turbulent model over predicts the experimental work. The convective heat transfer correlations provided for laminar and turbulent models were $Nu_m \propto Ra^{0.75}, Ra^{0.25}$, and a constant C respectively. With increasing Ra, the mode of heat transfer was found to change from heat conduction to natural convection. At Ra equals 1.3 x 10^9, convection dominates.

In the similar 2-D study by Lee et al [19] to analyze flow and heat transfer behaviors of a full-sized horizontal canister containing 21 fuel assemblies with helium as the working fluid, the peak temperature was found to be located in the second basket from the top along the vertical centerline. Increases in Ra can improve heat transfer resulting in systematically reduced temperatures for all components in the canister and allowing for a more uniform temperature field to be obtained as well (i.e., the average temperature difference between that of the basket surfaces and that of the inner surfaces of the canister decreases with the rise in Ra). The correlations provided to quantify heat transfer in the dry shielded canister were $Nu_m \propto Ra^{0.5}$ $(1.5 \times 10^6 - 1.0 \times 10^7)$ and $Ra^{0.25}$ $(1.8 \times 10^7 - 8.0 \times 10^7)$.

Lee et al [20] also conducted a 3-D numerical (CFD k-epsilon) and experimental studies on vertical concrete storage cask (half model) using FLUENT code. An initial validation was done by comparing the simulation with data from a testing cask containing a dummy fuel assembly (4.56 kW). Then, the cask containing 25.2 kW was simulated. The peak temperatures of the fuel rods were found to be around 300 ^{o}C, and nearly 80% of decay heat was transferred out of the cask by natural convection of air.

Tseng et al. [21] conducted similar work using FLUENT for a full-size vertical concrete cask of one-eighth (1/8) scale model, containing a stainless steel canister with 61 BWR fuel assemblies producing a total heat load of 18.3 kW. The fuel assembly was assumed as a homogeneous thermal model and its effective thermal conductivity was calculated in advance. Natural convection of helium in the canister is neglected and that of the air in the concrete gap was modeled using the Boussinesq method. It was concluded that the peak temperature is located in the middle of the central

assembly, which deviates from Lee's findings that the peak temperature is located at the upper part of the central assembly. Secondly, the change of the environmental temperature does not significantly affect the peak cladding temperature (only 13%) and the temperature difference between the central boundary fuel assembly. This could be induced by the neglect of natural convection.

In contrast to the ventilated concrete casks are the vertical non-ventilated steel casks frequently used commercially such as the TN-24P cask developed by Transnuclear Inc. The cask uses a resin-filled exterior shell and lid to isolate itself from the environment. A similar cask was tested and analyzed in the late 1980s by Creer et al [22]. With the availability of thermal experimental data, there is a resurging interest to study the thermal behaviors of such a cask to validate the simulations. A simulation of this cask was conducted by Yoo et al. [23] down to each individual fuel pin level to circumvent the use of effective thermal conductivity and porous media approximation for fuel assemblies, but for a small one eighth (1/8) scaled model by using FLUENT code with a total cell number of nearly 1.4 million. Brewster et al [24] analyzed a half (1/2) scaled model using a STAR-CCM+ CFD code with a total cell number up to 42.9 million. Both the simplified and high-resolution model provided predictions that are in good agreement with those from experiments.

Jei et al [25] also conducted a study of the thermal profiles of a vertical dry storage cask. For the study, a three-dimensional model of a vertical dry cask was constructed for simulation using FLUENT code. The cask contained a welded canister for 32 PWR used-fuel assemblies with a total decay heat load of 34 kW. An effective thermal conductivity model for a 17 x 17 PWR used fuel assembly was used in the simulation of thermal performance. The effects of internal pressure (1-6atm), canister fill gas (helium or nitrogen) and basket material (stainless steel or aluminum alloy) were analyzed to find the peak cladding temperature and cladding surface temperature. From the results, the thermal conductivity of the basket material enhances heat transfer and reduces peak cladding temperature. Natural convection was shown to affect peak cladding temperature (PCT) and canister surface temperature (CST), while the latter depends on the type of fill gas and canister internal pressure.

The major components modeled include a concrete overpack enclosed in carbon steel shells; a welded stainless steel multi-purpose canister (MPC); a cask lid and baseplate with radiation shielding provisions; air inlet and exit vents that provide passive cooling by natural convection (Figure 2.5).

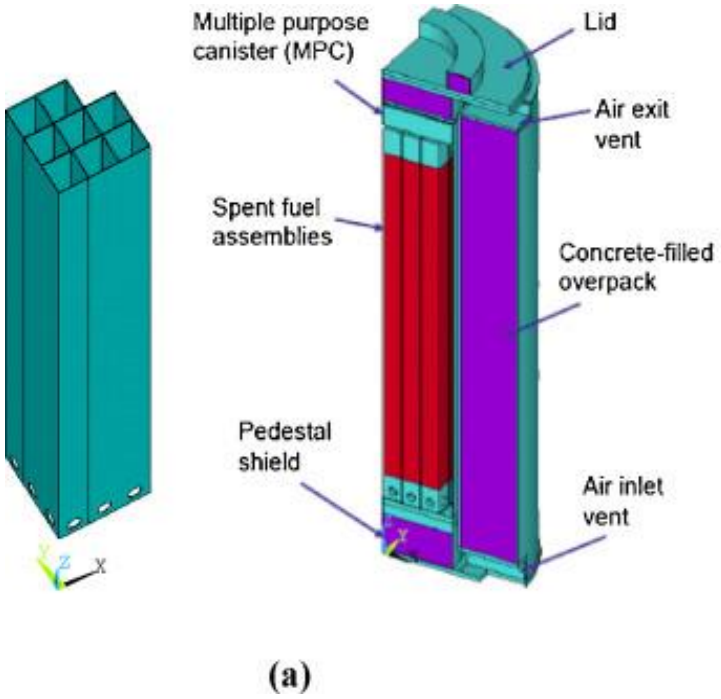

Figure 2.5: Components of the 3-D model by Jei et al [25]

For the analysis the total heat load of the cask, 34 kW was assumed to be uniformly distributed among the 32 PWR spent fuel assemblies with 1.0625 kW per assembly. For the simulation, it was shown that the peak cladding temperature of 387 ºC occurred in the spent fuel assembly near the center of the cask. Also, the velocity of air flow was higher at the air exit vent near the top of the vertical cask while air density was higher at the inlet vent near the bottom.

Jei et al [25] noted that the primary mechanisms for heat removal and passive cooling of the vertical storage cask were conduction through the spent fuel assemblies and the solid components, and natural convection inside and outside the canister. With the low flowrate of circulating gas, it is excepted that heat transfer by conduction trough a solid would be more effective than that by natural convection through gas. In analyzing the effects of basket materials and fill gas, Jei eat al. [25] considered the aluminum alloy Al-1100 and stainless steel, with Al-1100 having a thermal conductivity of 218 W/m K at 25 ºC, which is about 15 times higher than that of stainless steel. For

gases, helium and N_2 (air) were considered. The thermal conductivity of helium (0.142 W/m K) is about 5 times higher than that of N_2 (0.024 W/m K), both at 25 ^oC and ambient pressure.

Jei et al. [25] simulated the axial temperature profiles for the spent fuel assembly located near the center of the cask with three scenarios as shown in Figure 2.6: (1) a reference with 6-atm He inside the cask and stainless steel basket, (2) 6-atm N_2 inside the cask and a stainless steel basket, and (3) 6-atm N_2 and an Al-1100 basket. The results show that the calculated peak cladding temperature decreases from 387 ^oC (6 atm He) to 315 ^oC (6 atm N_2) with a stainless-steel basket to 190 ^oC with a N_2-filled cask and Al-1100 basket.

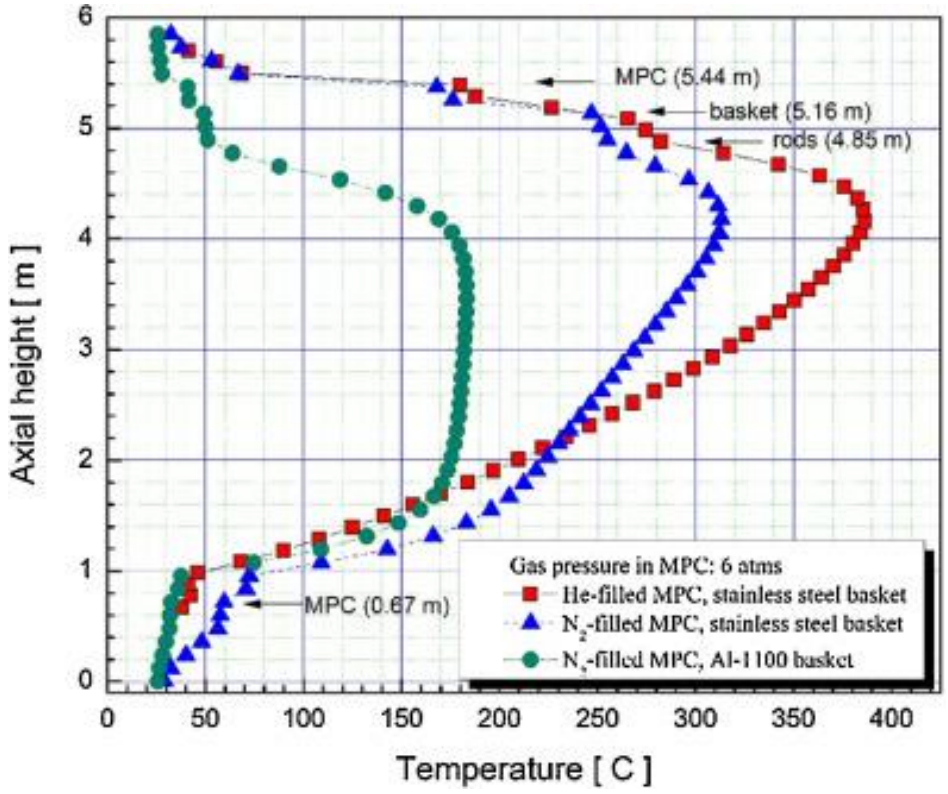

Figure 2.6: 3D simulation of axial temperature profiles for the spent fuel assembly located near the center of the cask under three scenarios by Jei et al [25]

Jei et al also simulated the radial temperature profiles for the same scenarios earlier mentioned, where the corresponding axial height is 4m above the fuel bottom. In the cases with the stainless-steel basket, the PCT decreased by about 70 ^oC and the peak basket temperature decreased

by about 100 ^{o}C at the axial location when the fill gas of He was replaced with N_2, both at 6 atm. The case with Al-1100 basket with 6 atm N_2 allowed for a drastic change in the calculated PCTs and peak basket temperatures. The PCTs of 190 ^{o}C stayed nearly the same for the spent fuel assemblies located near the center, middle and peripheral regions of the cask, while the basket temperatures remained flat near 60 ^{o}C from the center to the peripheral region of the cask. However, the difference in basket and cladding temperatures increased to about 130 ^{o}C. The work by Jei et al [25] showed that a stainless steel canister with a basket of high thermal conductivity material such as Al-1100 aluminum alloy drastically reduces PCT and CST. Also, the effects of N_2 fill gas on the PCT and CST and are also dramatic. The implication here is that changing canister fill gas from He to N_2 should be relatively easy for any vertical cask design. Although N_2 is not as inert as He, it can provide a non-oxidizing environment inside the canister during extended long-term storage and subsequent transportation of high burnup fuel.

From the studies done on dry casks as discussed, there is cause to reason that with increasing Ra, the mode of heat transfer changes from heat conduction to natural convection. Noting that at Ra = 1.3×10^9, convection dominates. Nishimura et al [18] showed in their study that one fifth (1/5) of an actual dry shielded canister generated Rayleigh numbers varying from $3x10^7$ to $2x10^8$. Given that length is a major property in calculating Ra, larger Ra values will be expected for larger-scale models and in full-size casks. There is ongoing work to obtain realistic, temperature estimates for dry storage components over time, therefore reasonable assumptions will have to be made in the experimental work, modeling and numerical work of used fuel bundles and dry storage components.

This work will, therefore, analyze the mode of heat transfer present in a cold plated cask for use PWR fuels.

CHAPTER 3: Experimental Procedures

Sakae casting manufactured and supplied four cold plates each measuring 8 by 65 inches with a thickness of 0.56 inches. This translates to approximately to a 1/3 scaled model by height of full fuel bundle assembly which generally stands at 4 m tall and 21 cm wide. These cold plates are so-called because they each have 2 U-tubes cast in them spanning the length of the plate with an inner diameter of about 3/8 inches and a 15/32 outer diameter (Figure 3.1). Cold water will enter one leg of each U-tube while hot water exits from the second leg of the U-tube. It is essential to note that the proprietary casting method employed by Sakae casting creates a negligible clearance between the tubing and the slabs. This goes to support the assumption that each slab with the tubing forms a single body instead of having two plates and tubes bonded, screwed or welded together. Further discussion on this is included in the theoretical analysis.

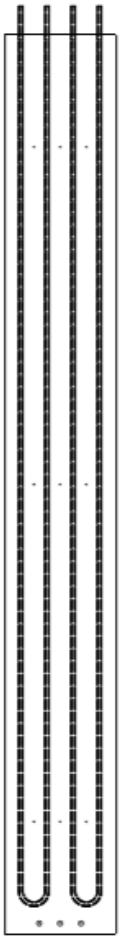

Figure 3.1: Diagram of Sakae Cold Plate

With the use of 0.25-in angle irons, the plates were put together to form the basic frame of the cask as shown in Figure 3.2. A stainless-steel cap was manufactured to accommodate the tubes protruding from the top of the slabs, a central tube through which thermocouples can be fed into the cask, and threaded holes that allow for insertion heaters to be fitted in each quadrant of the cask as illustrated in Figure 3.3 and Figure 3.5.

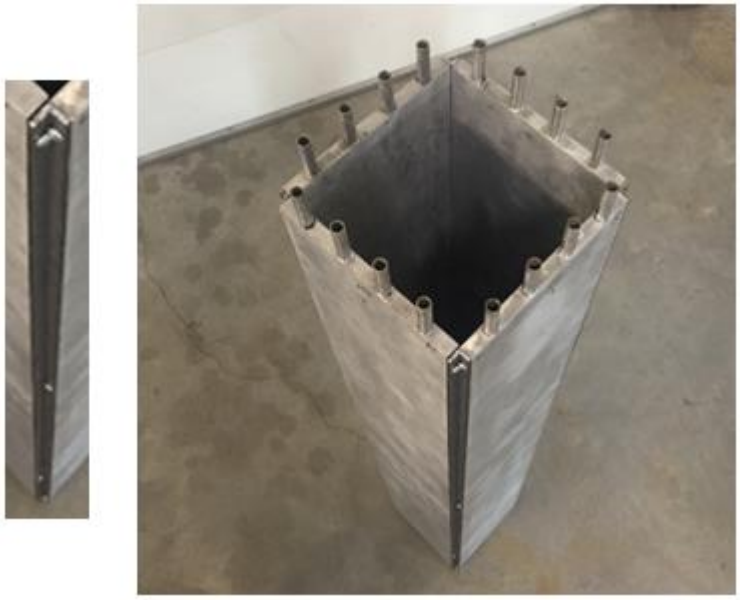

Figure 3.2: Figure showing basic frame of Sakae experimental cask constructed with 0.25-in angle irons

To facilitate discussion about the cask, the following labeling will be used to describe the sides: S1, S2, S3, and S4 (Figure 3.3). The insertion heaters used were ¾ inches in diameter with a heated length of 61 inches. These heaters rated at 220 V and 1500 W each were placed in the cask such that they were 2 inches from the bottom of the cask. Six thermocouples were fed into the cask through the central tube such that a pair of thermocouples corresponded to a defined top, the middle and bottom level of the cask as illustrated in Figure 3.4. From the top of the cask, the levels measure 10, 35 and 60 inches respectively. Each thermocouple pair labeled A and B is set up such that lead "A" is pointed to S1 while lead "B" is pointed to S4. The thermocouple leads were extended so that their ends were in line with the centers of the heaters as depicted in Figure 3.3 and Figure 3.6.

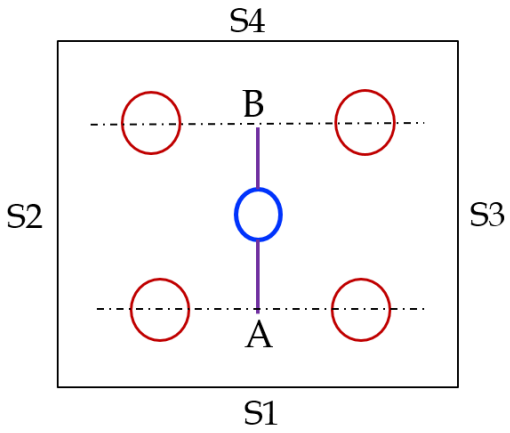

Figure 3.3: Schematic diagram of the top view of the cask, showing the heaters in each quadrant, the central instrumentation and positioning of the thermocouples

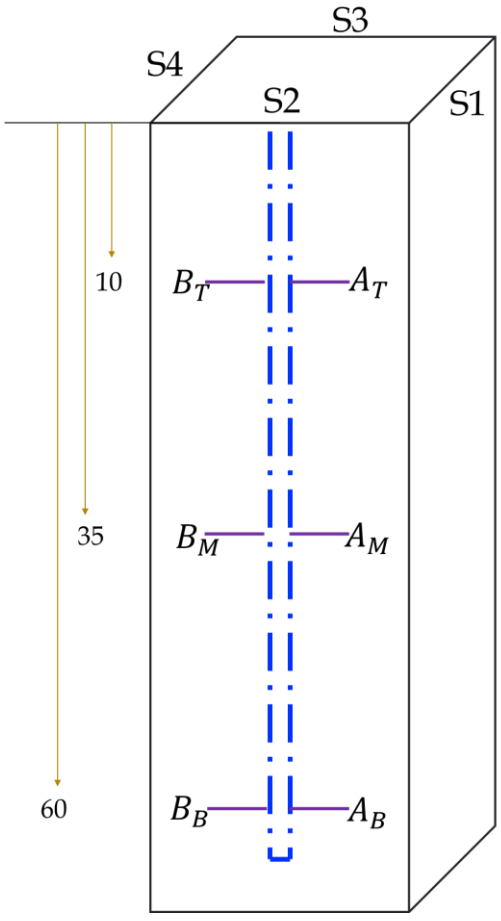

Figure 3.4: Schematic of the internal layout of the thermocouples

Figure 3.5: Cask with slab S1 taken off showing the insertion heaters and central thermocouple tube

Figure 3.6: Image of internal thermocouple setup

The thermocouples on the outer walls were center-punched into the slabs and arranged such that there were 8 of them on each cask level (top, middle, and bottom); one each on S1 and S4, and 3

each on S2 and S3 as illustrated in Figure 3.7 and Figure 3.8. The outer frame was built around the cask unto which hoops were mounted to allow easy supply and drainage of water to the system as shown in Figure 3.9. The cask was then insulated to ensure a negligible loss of heat through the cask walls to the environment as shown in Figure 3.10.

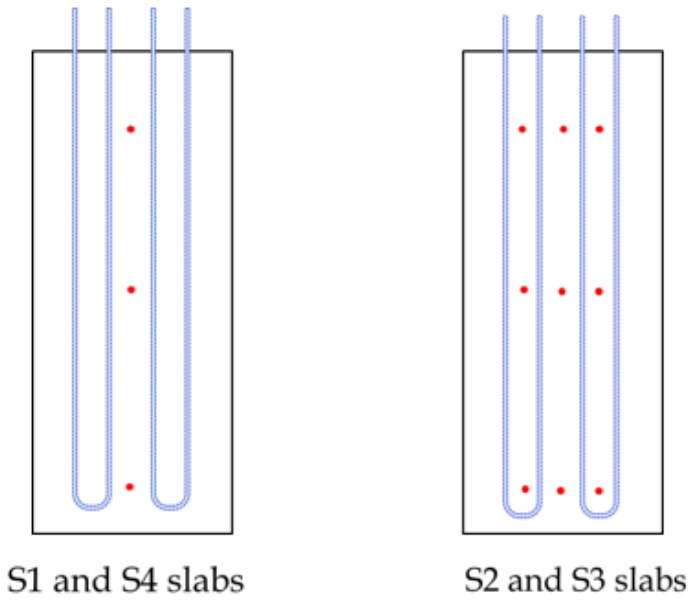

Figure 3.7: Schematic of the layout of thermocouples on the outside of the slabs

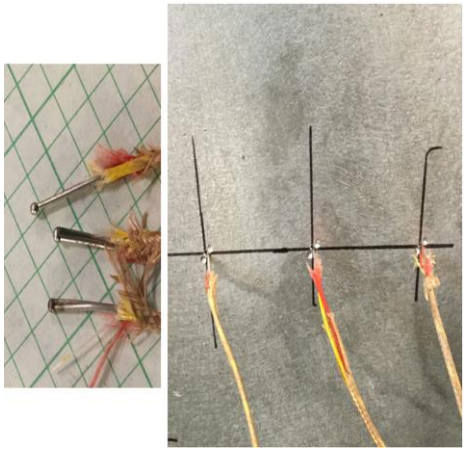

Figure 3.8: Thermocouples center punched into the slabs

Figure 3.9: Image of water supply hoops

Figure 3.10: Image of insulated cask

With the construction complete, the heaters were connected to rheostats that produce a constant heater surface temperature at defined temperature levels. Experiments were conducted at different heater temperature levels long enough for the measured cask internal temperatures to be at equilibrium as reported in Table 3.1. Data collection at equilibrium was essential to support steady-state assumptions during theoretical analysis. Flow rate of water for each temperature level remained at a constant 6.3 gpm.

Table 3.1: Showing the equilibrium duration of each temperature level and the time to reach equilibrium from the start of each run

Heater temp. (ºC)	**Run time (min)**	**Equilibrium duration (min)**	**Time to Equil. (mins)**
100	68	50	19
150	79	61	17
200	76	57	19
300	72	49	22
400	78	58	20
500	127	108	19
600	224	201	23

CHAPTER 4: Experimental Results

As earlier mentioned, each test run was conducted in steps of heater surface temperatures regulated by the rheostats. The tests were not terminated until internal air and slab average temperatures reached and maintained equilibrium for a considerable amount of time. Figure 4.1 is a plot illustrating the temperature step increase as explained.

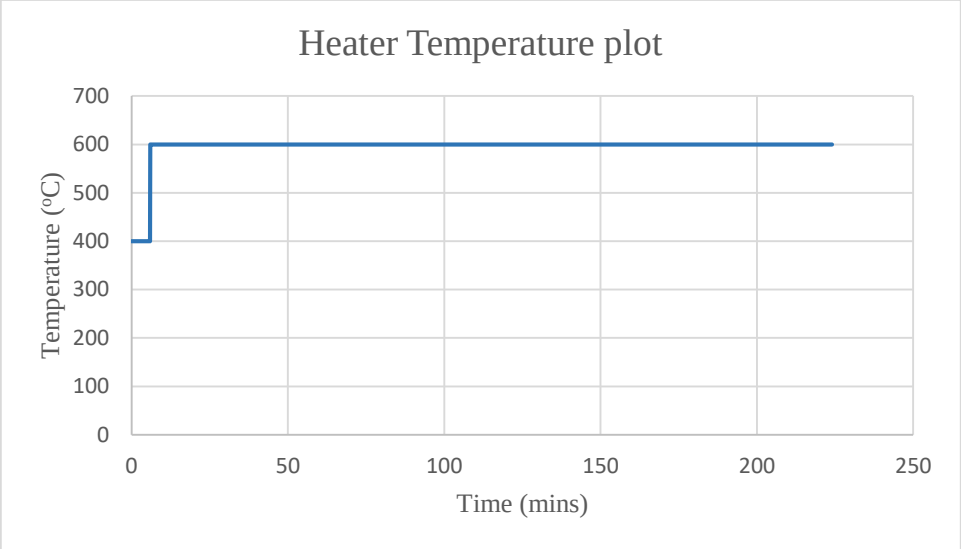

Figure 4.1: Plot showing heater temperature step

Figure 4.2, Figure 4.3, and Figure 4.4 are plots showing the build-up to, and duration of equilibrium before the test at the 600 °C heater temperature was terminated. Table 4.1 and Table 4.2 are a summary of the water outlet temperatures, average cask internal air temperatures and the outer plate temperatures recorded for each test run. In Table 4.2, the number of the thermocouples (TCs) over which the averages listed were calculated are given in parenthesis. Table 4.3 lists the standard deviations associated with the calculated averages. The deviations in the internal temperatures are higher in account of the temperature difference between the thermocouples at the top section of the cask (higher readings) and those at the bottom (lower readings). Note that the inlet and outlet water temperatures in Table 4.1 are recorded from single thermocouples and therefore not an average value.

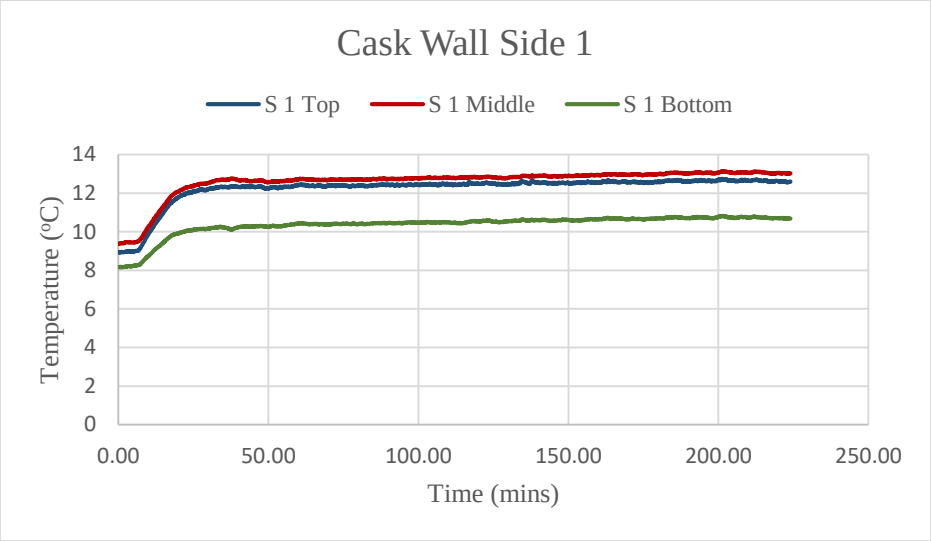

Figure 4.2: Slab S1 temperature profiles at 600 °C heater temperature

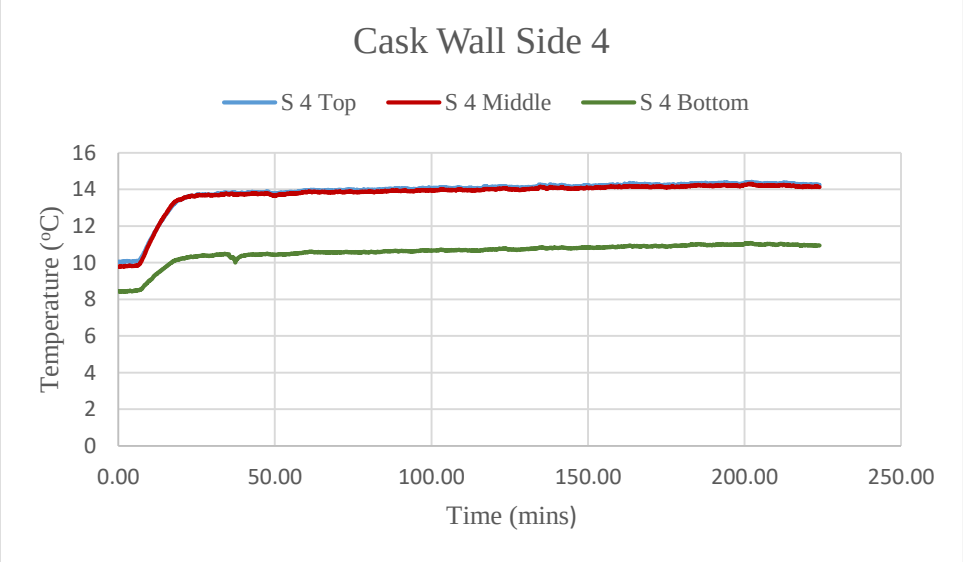

Figure 4.3: Slab S4 temperature profiles at 600 °C heater temperature

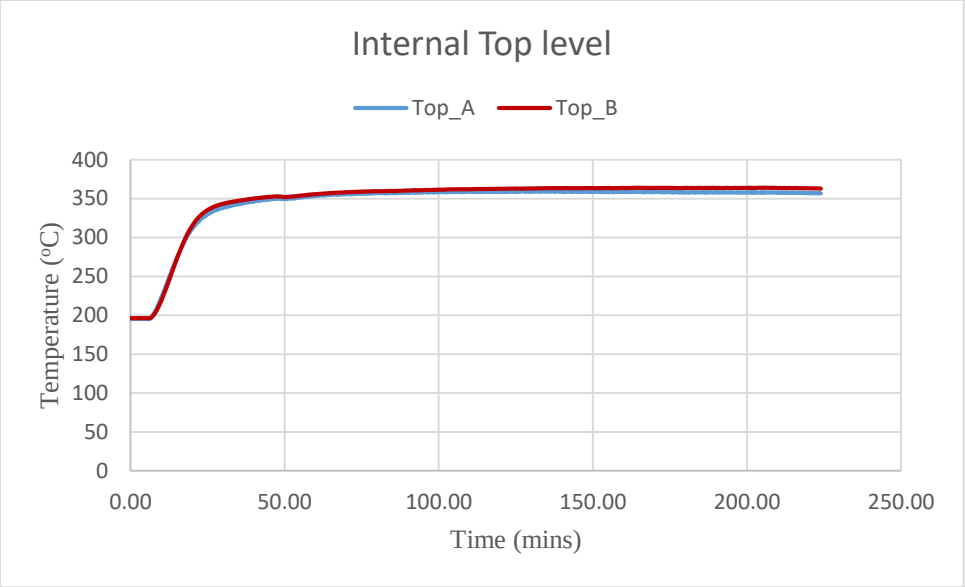

Figure 4.4: Plot showing internal air temperature profiles at 600 oC heater temperature (Top level is 10in below the top edge of the plate).

Table 4.1: Recorded water temperatures at equilibrium

Heater Temp. (°C)	**Water Temp. °C**	
	Inlet	**Outlet**
100	7.36	18.87
150	7.36	19.72
200	7.36	17.07
300	7.36	17.87
400	7.36	17.43
500	7.36	20.21
600	7.36	19.32

Table 4.2: Recorded internal air and outer wall temperatures at equilibrium

Heater Temp. (ºC)	Internal Air Temp. (ºC)			Outer Wall Temperature (ºC)				
	Internal A	Internal B	Average (6 TCs)	Side 1 (3 TCs)	Side 2 (9 TCs)	Side 3 (9 TCs)	Side 4 (3 TCs)	Average (24 TCs)
100	31.29	30.52	30.90	7.78	7.88	7.61	7.91	7.80
150	31.29	30.52	30.91	7.96	7.88	7.61	7.91	7.84
200	61.38	58.82	60.10	7.94	8.13	7.78	8.07	7.98
300	98.73	95.29	97.01	8.63	8.82	8.35	8.98	8.69
400	139.52	132.15	135.84	9.02	9.13	8.62	9.45	9.06
500	198.97	184.05	191.51	10.64	10.94	9.31	11.43	10.58
600	260.72	244.66	252.69	12.09	12.44	12.11	13.17	12.45

Table 4.3: Recorded internal air and slab temperatures with standard deviations

Heater Temp. (ºC)	Internal Air Temp. (ºC)		Outer Wall Temperature (ºC)	
	Average (6 TCs)	St. Dev.	Average (24 TCs)	St. Dev.
100	30.90	14.10	7.8	0.28
150	30.91	14.11	7.84	0.29
200	60.10	30.09	7.98	0.33
300	97.01	48.74	8.69	0.52
400	135.84	77.49	9.06	0.72
500	191.51	101.38	10.58	2.15
600	252.69	151.09	12.45	1.25

With these recorded values, the Churchill and Chu correlation was used to calculate the average heat transfer coefficient at the walls of the cask. The exact equation and the process used is discussed in Chapter 5. Table 4.4 provides a summary of the calculated average heat transfer coefficients. The columns labeled “at high” and “at low” correspond to the heat transfer coefficient values calculated at plus and minus the standard deviations (St.Dev) of the slab temperatures respectively.

Table 4.4: Calculated average heat transfer coefficients at the cask walls. "at high" and "at low" correspond to values calculated at plus and minus the standard deviations (St.Dev) of the slab temperatures

Slab Temp. (ºC)		**h (W/m^{2}K)**			
Avg (24 TCs)	**St.Dev**	**at Agv.**	**at high**	**at low**	**St. Dev**
7.77	0.28	4.01	4.60	3.02	0.80
7.79	0.29	4.01	4.60	3.02	0.80
8.64	0.33	5.01	5.61	3.91	0.86
8.64	0.52	5.73	6.31	4.67	0.83
8.97	0.72	6.21	6.78	4.95	0.93
10.35	2.15	6.63	7.08	5.57	0.77
12.36	1.25	6.92	7.29	5.70	0.83

CHAPTER 5: Discussion

5.1 Theoretical analysis

The amount of energy removed from the cask was calculated using the basic internal fluid convection equation given by;

$$\dot{Q}_{water} = m\ cp\ (T_i - T_o) \quad (1)$$

Where the flow rate "*m*" is 6.3 gpm (0.397 kg/s) and the specific heat "*cp*" is the 4200 J/kg-K, the energy removed by water exceeds the combined rating of the electric heaters (6 kW) by about three times as show in Table 5.1.

Table 5.1: Calculated power removed by water from experimental data

Heater Temp. (ºC)	**Water Temp. (ºC)**		**Q water (kW)**
	Inlet	Outlet	
100	7.36	18.87	19.19
150	7.36	19.72	20.60
200	7.36	17.07	16.19
300	7.36	17.87	17.52
400	7.36	17.43	16.79
500	7.36	20.21	21.42
600	7.36	19.32	19.94

To address the anomaly in the recorded water outlet temperatures, an energy balance equation was used to calculate the combined heater power at each temperature level (T_r) , along with the associated heat transfer coefficients at the heater (h_r) and slab (h_s) surfaces given by:

$$\dot{Q}_{total} = \dot{Q}_{conv} + \dot{Q}_{rad} = \dot{Q}_{water} \quad (2)$$

Fundamental assumptions employed included the following. One dimensional steady-state conditions within the cask, a constant flow rate of water through the cold plates, constant and symmetrical distribution of heat flux within the cask, all the heat from the heaters is transferred

directly into the water with negligible heat loss through the top or bottom of the cask, and that the heat loss from the cask walls to the environment is negligible. Also, as earlier mentioned it is assumed that there are no gaps between the tubes and the plate. This assumption eliminates the need to consider air pockets within the plates during the theoretical analysis thereby neglecting radiation heat transfer between the slab and tubing. Furthermore, the slab material used in this analysis is Aluminum with thermal conductivity of 236 W/m-K while the tubing material is 304 stainless steel with a thermal conductivity of 14 W/m-K.

The governing resistance network involved a heat transfer rate from the heater to the cask slab by radiation, with convective heat transfer from the heater rods to the air and from the air to the slab. The governing equations for the study included the following.

$$\dot{Q}_{rad} = A_r \varepsilon \sigma (T_r{}^4 - T_s{}^4) \tag{3}$$

$$\dot{Q}_{conv} = h_r A_r (T_r - T_{air}) = h_s A_s (T_{air} - T_s) \tag{4}$$

Where the subscripts *r* and *s* represent the heater and slab surfaces respectively. The slab temperature is assumed to equal to the tubing temperature, due to the negligible resistance through the aluminum, supported by this brief analysis.

For the analysis, a 4-m tall cylindrical UO_2 fuel core is considered. The core diameter used is 24-cm; being similar to a PWR fuel bundle width of 21 cm. The core is layered with 10 cm thick aluminum metal and 24 cm thick concrete (Figure 5.1). The analysis is done with Equations (5) to (10) as the governing equations.

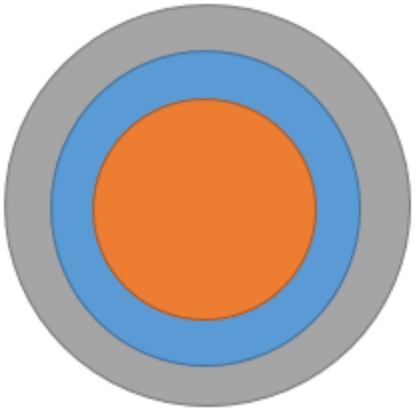

Figure 5.1: Top cross-sectional view of concentric cylinders with fuel in the middle, layered with aluminum and then concrete

$$T_{max} - T_{\infty} = \frac{q'}{2\pi}\left[\frac{1}{2k_f} + \frac{1}{k_{Al}} ln\left(\frac{R_{Al}}{R_f}\right) + \frac{1}{k_c} ln\left(\frac{R_c}{R_{Al}}\right) + \frac{1}{R_c h_g}\right] \quad (5)$$

$$T_{fo} = T_{max} - \frac{q'}{4\pi k_f} \quad (6)$$

$$T_{Al} = T_{fo} - \frac{q'}{2\pi k_{Al}} ln\left(\frac{R_{Al}}{R_f}\right) \quad (7)$$

$$T_c = T_{Al} - \frac{q'}{2\pi k_c} ln\left(\frac{R_c}{R_{Al}}\right) \quad (8)$$

$$T_c = T_{Al} - \frac{q'}{2\pi k_c} ln\left(\frac{R_c}{R_{Al}}\right) \quad (9)$$

$$h_g = \frac{Q}{A(T_c - T_{\infty})} \quad (10)$$

$$\lambda\,[\mathrm{W/(m\cdot K)}] = \frac{100}{7.5408 + 17.692\tau + 3.6142\tau^2} + \frac{6400}{\tau^{5/2}}\exp\left(\frac{-16.35}{\tau}\right)$$

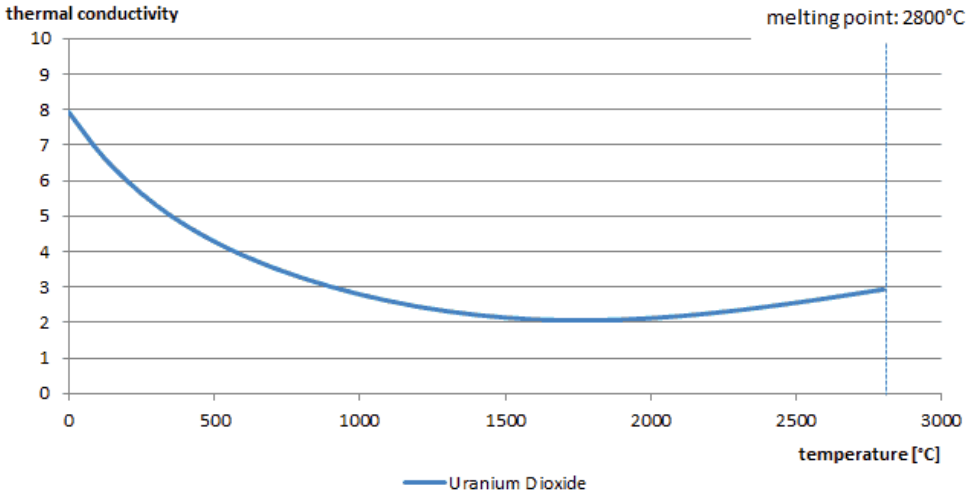

Figure 5.2: Thermal conductivity of UO_2 with a density of 95% [26]

The thermal conductivity correlation shown in Figure 5.2, was used for the fuel core, where $\tau = T_{max}/1000$. The uncertainty of this correlation is +10% in the range of 298.15 to 2000 K and +20% in the range of 2000 to 3120 K [26].

The convective heat transfer coefficient of air flow can be approximated as [27]

$$h_c = 10.45 - v + 10v^{1/2} \tag{11}$$

where v is the relative speed between the object surface and air. This being valid for $2 \geq v \leq 20\ m/s$.

Figure 5.3 shows a plot of the temperature profiles for the aluminum and concrete cask at 3 m/s airflow velocity. It is observed that with the aluminum thickness of only 10 cm, conductive resistance through this material is almost negligible. From the analysis, the thickness of aluminum would have to be at least 50 cm to result in a 1-degree difference in temperature between the aluminum outer surface and the core surface. Other deductions include the following: increasing the heat transfer coefficient of airflow reduces the concrete temperature and a unit increase in the ambient temperature (T_∞) increases all temperatures by 1 unit.

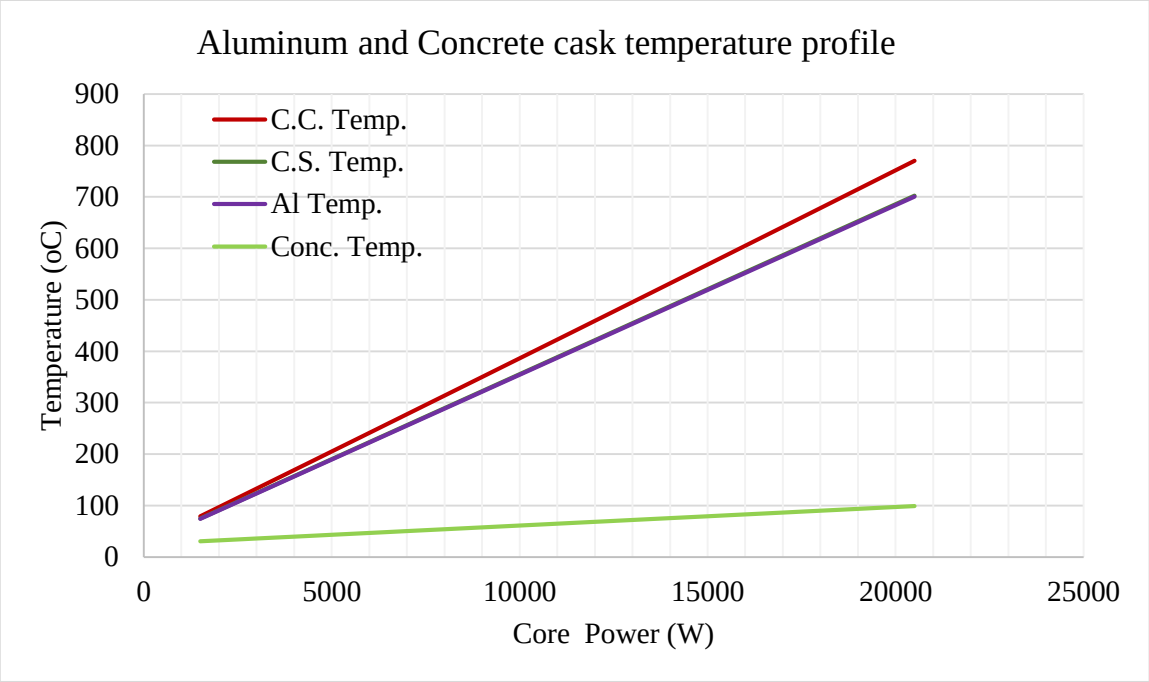

Figure 5.3: Temperature plots of aluminum and concrete cask. C.C. is Core Centerline, C.S. is core surface, Al is Aluminum and Conc. is concrete

Going back to the energy balance equation within the cask, h_s for each heater temperature level was calculated with the Churchill and Chu correlation given by:

$$\overline{Nu_L} = \frac{\bar{h}L}{k} = \left\{ 0.825 + \frac{0.387 {Ra_L}^{1/6}}{\left[1 + (\frac{0.492}{Pr})^{9/16}\right]^{8/27}} \right\}^2 \tag{12}$$

The general correlation recommended by Yang for laminar and turbulent regions was used to calculate h_r [28]. This is given by:

$$Nu_L = \left\{ 0.60 \left(\frac{L}{D}\right)^{0.5} + 0.387 \left[\frac{Ra_L}{[1 + (0.492/Pr)^{9/16}]^{16/9}} \right]^{1/6} \right\}^2 \tag{13}$$

This equation was used because the geometry of the heaters did not meet the criterion necessary for them to be treated as a vertical plate given by:

$$\frac{D}{L} \geq \frac{35}{{Gr_L}^{1/4}} \tag{14}$$

Table 5.2 summarizes the resulting power from the energy balance with a 6-kW combined output limit. The losses shown are calculated as a ratio of the top and bottom plate areas to the area of the side walls which amount to a 6.15% uncertainty in the calculated power output. Table 5.3 and Table 5.4 present a summary of the resulting outlet water temperatures, air temperatures and the calculated heat transfer coefficients at the rod and the slab surfaces. The assumed inlet water temperature used is 7.36 °C. These results show a more consistent heat transfer network as the water outlet temperature is less than the slab temperature, which is in turn less than the air temperature, which is also less than the heater temperature. It is also observed that (h_r) is almost twice as high as (h_s). This is attributed to the significant difference in film temperatures at the rod and slab surfaces.

Table 5.2: Summary of calculated heater power in the 65-in tall cask using data from the experiment with associated uncertainty

		Total	**Loss to**	**Total loss**	**Uncertainty**
Measured	**Power output per heater (W)**	**power to cask walls**	**top or bottom plate**	**to top and bottom**	**in heater power**
Surf. Temp		**4xQ (W)**	**(W)**	**(W)**	**(%)**
100	46.63	186.53	5.74	11.48	6.15
150	78.43	313.73	9.65	19.31	6.15
200	118.76	475.06	14.62	29.23	6.15
300	224.97	899.87	27.69	55.38	6.15
400	392.67	1570.70	48.33	96.66	6.15
500	665.89	2663.56	81.96	163.91	6.15
600	1099.35	4397.40	135.30	270.61	6.15

Table 5.3: Summary of calculated total power supplied with the resulting outlet water temperatures. Temperatures in (°C)

T rod	Q total (W)	ΔT water	Tout
100	186.53	0.11	7.47
150	313.73	0.19	7.55
200	475.06	0.28	7.64
300	899.87	0.54	7.90
400	1570.70	0.94	8.30
500	2663.56	1.60	8.96
600	4397.40	2.64	10.00

Table 5.4:Sumary of calculated air and slab temperatures with corresponding heat transfer coefficients at the rod and slab surfaces

Q total (W)	T air	T slab	h rod	h slab
186.53	38.42	7.77	8.07	4.35
313.73	51.76	7.79	8.32	4.82
475.06	70.17	8.64	9.17	5.25
899.87	101.86	8.64	9.93	5.80
1570.70	133.57	8.97	10.45	6.19
2663.56	167.73	10.35	10.95	6.46
4397.40	202.69	12.36	11.34	6.92

5.2 Sakae's cask for full scale (17X17) PWR fuel bundle

The analysis for the full cask was done in two ways. The first approach used the same heater power calculated for the 65 in tall cask, with the only difference being the height (4 m). While, the second approach used decay heat values obtained from a study done at Oak Ridge National Lab.

Table 5.5 summarizes the calculated temperatures and heat transfer coefficients for the 4-m tall cask where the total power output is the same as the power output in the 65-in tall cask. Given the new length of the heaters, they have a reduced surface temperature, ranging from 99 °C to 491 °C. Assuming that the power produced is absorbed into the water, then the outlet water temperature values remain the same as those calculated in the shorter cask. Air and slab temperatures were

calculated ranging from 19 ^{o}C to 181 ^{o}C and 7.43 ^{o}C to 9.03 ^{o}C respectively, in accordance with the established energy balance from the heaters to the slab. Lower heat transfer values were calculated owing to the height of the heaters and cask ranging from 6.57 to 8.63 W/m^{2}K at the rod surface and 3.27 to 4.06 W/m^{2}K at the slab surface. As with the shorter cask, the heat transfer coefficients at the heater surface were about twice as high as the calculated values at the slab surface.

Table 5.5: Summary of calculated heater rod, air and slab temperatures with corresponding heat transfer coefficients at the rod and slab surfaces for 4m tall cask

Q total (W)	T rod	T air	T slab	h rod	h slab
186.53	99	19.32	7.43	6.57	3.27
313.73	147	53.73	7.48	6.58	3.56
475.06	194	68.44	7.54	6.75	3.68
899.87	269	94.13	7.70	7.40	3.93
1570.70	322	117.79	7.96	8.06	3.92
2663.56	422	154.67	8.37	8.29	3.95
4397.40	491	180.53	9.03	8.63	4.06

For the second approach, Ade et al [29] from the Oak Ridge National Laboratory (ONL) conducted a study to calculate decay heat for PWR and BWR Assemblies fueled with Uranium and Plutonium Mixed Oxide Fuel using the SCALE code system. Specifically, the SCALE/TRITON sequence was used for depletion calculations and SCALE/OREGEN-ARP was used for calculation of decay heat rates as a function of specific initial fuel composition and discharge burnup level.

Two fuel bundle models were chosen to represent common fuel bundles used in commercial nuclear power reactors. For the PWR, the ORIGEN-ARP template for Westinghouse 17x17 fuel bundle was chosen from the SCALE distribution. For the BWR a 7X7 fuel assembly model was used analyzed.

The numerical analysis in this work is concerned with the data obtained from the PWR fuel bundle study by Ade et al. The major modeling dimensions used in their study are shown in Table 5.6.

Table 5.6: PWR 17x17 fuel bundle dimensions (centimeters)[29]

Assembly pitch	21.4030
Fuel rod pitch	1.2590
Fuel pallet radius	0.4025
Fuel gap radius	0.4110
Fuel clad radius	0.4750
Guide tube inner radius	0.5718
Guide tube outer radius	0.6121

For this model by Ade et al [29], no intra-assembly gap was modeled, and no burnable absorbers were used. The model uses as nominal moderator density of 0.72 g/cm^3 with a soluble boron concentration of 600 ppm by weight. A SCALE/NEWT figure of the PWR model is shown in Figure 5.4.

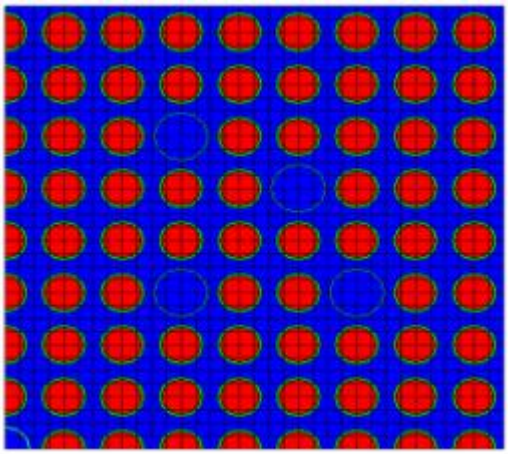

Figure 5.4: SCALE/NEWT 1/4 assembly model of the PWR 17x17 fuel bundle [29]

As part of the fuels analyzed by Ade et al [29] was UO_2 at discharge burnups of 35, 40, 45 and 50 GWd/MTHM. Ade et al included the raw data resulting from their study in their report from which the decay heat used in this numerical work was gathered as shown in Table 5.7.

Table 5.7: Decay heat data as a function of time after shutdown of PWR fuel bundle for 50 GWd/MTHM obtained from the study by Ade et al [29]

Age (yrs.)	Decay heat (W/MTHM)
1	11370
2	7116
3	4549
4	3343
5	2850
6	2440
7	2240

A bundle weight of 0.46 tons [29] was multiplied by the decay heat to obtain the fuel bundle power as shown in Table 5.8. A homogeneous distribution of heat flux within the bundle is assumed for this analysis. The dimensions for slab used for this analysis are 4-m by 9.75-in, with the same plate thickness, pipe diameters, and inlet water temperature as with earlier analyses. After iteratively solving the energy balance equations such that convection from the bundle is equal to the convection to the slab surface, and that that the sum of heat output by radiation and convection is limited to the obtained decay heat values, the values summarized in Table 5.8 and Table 5.9 were the temperatures and heat transfer coefficients calculated.

Table 5.8: Summary of cask temperature values (°C) for the decay heat gathered from the ONL study

Age (yrs.)	Q total (W)	T rod	T air	T slab	ΔT water	Tout
7	1030	198	75.67	7.75	0.62	7.98
6	1122	209	79.74	7.78	0.67	8.03
5	1311	235	89.19	7.86	0.79	8.15
4	1538	259	97.77	7.93	0.92	8.28
3	2093	313	117.52	8.14	1.26	8.62
2	3273	389	140.28	8.59	1.96	9.32
1	5230	477	171.51	9.93	3.14	10.50

Table 5.9: Summary of heat transfer coefficients (W/m^2K) within the cask for the ONL data

Q total (W)	h bundle	h slab
1030	7.72	3.45
1122	7.83	3.52
1311	7.98	3.62
1538	8.04	3.65
2093	8.05	3.67
3273	8.06	3.85
5230	8.08	4.00

As expected with the actual bundle, the higher decay heat values result in higher air and slab temperatures within the cask. Heat transfer coefficients at the bundle surface ranged from 8.08 W/m^2K in the first year to 7.72 W/m^2K in the seventh year after fuel discharge. Calculated heat transfer coefficients at the slab surface ranged from 4 W/m^2K in the first year to 3.45 W/m^2K in the seventh year after discharge from the reactor.

CHAPTER 6: Conclusion

In the present study, experimental and numerical work has been performed to explore the thermal behavior of a proposed storage cask for used LWR fuels. The idea of the cask is to capitalize on cold plate technology being used in various industries to tackle the issue of used nuclear fuel storage which is fast approaching criticality in nuclear power-producing countries around the world. For the experimental study, four electric heaters were inserted into the cask and run at temperatures in hundred-degree increments from 100 ^{o}C to 600 ^{o}C. This set up represented approximately a one-third scale model of an actual fuel assembly. Water is then supplied to the cask at 7.36 ^{o}C and at a rate of 6.3 gpm. This flow is distributed to 8 inlet cold plate tubes and each test is allowed to run until equilibrium of internal air and slab temperatures. It is observed that the minimum and maximum water outlet temperatures are 17 ^{o}C and 20 ^{o}C at the 200 ^{o}C and the 500 ^{o}C levels respectively, although there is a general slow rise in water outlet temperature between temperature steps. It is also observed that the slab average temperature realized a steady increase from 8 ^{o}C to 12.4 ^{o}C. Using the Yang, and Churchill and Chu correlations for heat transfer at vertical cylinders and vertical plates respectively, and the data from the experiments, the heat transfer coefficients at the slab for the runs ranged from 4.01 to 6.92 W/m^{2}K.

Numerical work was done for the 1/3 scaled model which resulted in calculated heat transfer coefficients at the heater surface ranging from 8.07 to 11.34 W/m^{2}K and from 4.35 to 6.92 W/m^{2}K at the slab surface. To understand the effect a change in height will have on the heat transfer of the cask, a comparison between a 65-in tall cask and a 4-m tall cask was done with the same heater power and heater surface temperature conditions. At 4-m tall, the heat transfer coefficients ranged from 6.57 to 8.63 W/m^{2}K at the heater surface and from 3.27 to 4.06 W/m^{2}K at the slab surface.

Finally, a case was considered where a 17x17 PWR fuel bundle is cooled in the cask with decay heat values obtained from a study by Ade et al [29]. A homogeneous distribution of heat flux within the bundle was assumed and the bundle temperature assumed to be the temperature per rod. The calculated heat transfer coefficients in the cask ranged from 8.08 to 7.72 W/m^{2}K at the heater surface and from 4 to 3.45 W/m^{2}K at the slab surface. The higher heat transfer coefficients for the bundle analysis correspond to a one-year-old fuel while the lower value corresponds to a seven-year-old fuel.

REFERENCES

[1] P. Adelfang, A. J. Soares, and Agence internationale de l'énergie atomique, *Corrosion of research reactor aluminium clad spent fuel in water*. Vienna: International Atomic Energy Agency, 2009.

[2] F. Carré and J.-M. Delbecq, "Overview on the French Nuclear Fuel Cycle Strategy and Transition Scenario Studies," *Revue Générale Nucléaire*, no. 6, pp. 95–101, Nov. 2009.

[3] T. P. Lagus and W. Intern, *Reprocessing of Spent Nuclear Fuel: A Policy Analysis*. 2005.

[4] Y. P. Zhang, X. L. Yu, Q. K. Feng, and R. T. Zhang, "Thermal performance study of integrated cold plate with power module," *Applied Thermal Engineering*, vol. 29, no. 17, pp. 3568–3573, Dec. 2009.

[5] G. Hildenbrand, "Atomwirtschaft 29," p. 414, 1984.

[6] M. Peehs, W. Petrie, H. P. Fuchs, and F. Schlemmer, "Long term storage behaviour of spent LWR fuel," *Proc. NEA-Seminar Storage of Spent Fuel Elements, Madrid*, p. 223, Jun. 1978.

[7] M. Peehs, W. Jung, G. Kasper, and F. Schlemmer, "Long term storage behaviour of spent LWR-fuel," *Proc. Patram 80, Berlin, Vol. II (1980)*, p. 934.

[8] D. P. Ross, "Yucca Mountain and Reversing the Irreversible: The Need for Monitored Retrievable Storage in a Permanent Repository Symposium: The Environmental Law of War: Note," *Vt. L. Rev.*, vol. 25, no. 3, pp. 815–852, 2001 2000.

[9] G. Kasper, M. Peehs, J. Fleisch, and H. Unger, "Dry storage instrumented bundle experiments," *Nuclear Energy Agency of the OECD (NEA): OECD*, 1982.

[10] M. Peehs, E. Steinberg, D. Jorde, and H. Schonfeld, "Zircaloy post-pile creep: Experimental procedure, test samples and first results," 1983.

[11] M. Peehs and J. Fleisch, "LWR Spent Fuel Storage Behaviour," *Journal of Nuclear Materials*, vol. 137, no. 3, pp. 190–202, Feb. 1986.

[12] G. Kasper, M. Peehs, and E. Steinberg, "Experimental Investigation of Post-pile Creep of Zircaloy-cladding tubes," *paper submitted to 8th Int. SMiRT Conf., Brussels*, p. 1986.

[13] "Hansen et al., 2012 B. Hansen, et al. Gap Analysis to Support Extended Storage of Used Nuclear Fuel Rev. 0 FCRD-USED-2011-000136 (January, 2012)." .

[14] M. Billone, T. Burtseva, Z. Han, and Y. Liu, "Effects of Multiple Drying Cycles on High-Burnup PWR Cladding Alloys," ANL-14/11, 1159911, Sep. 2014.

[15] "Chopra, 2014 O. K. Chopra et al. (2014). Managing aging effects on dry cask storage systems for extended long-term storage and transportation of used fuel. Fuel Cycle Research and Development, FCRD-UFD-2014-000476, Prepared for U.S. Department of Energy Used Fuel Disposition Campaign, Sept. 2014." .

[16] "NRC: News Releases." [Online]. Available: https://www.nrc.gov/reading-rm/doc-collections/news/. [Accessed: 28-Oct-2019].

[17] X. Heng, G. Zuying, and Z. Zhiwei, "A numerical investigation of natural convection heat transfer in horizontal spent-fuel storage cask," *Nuclear Engineering and Design*, vol. 213, no. 1, pp. 59–65, Apr. 2002.

[18] M. NISHIMURA, H. SHIBAZAKI, S. FUJII, and I. MAEKAWA, "Natural Convection Heat Transfer in the Horizontal Dry Storage System for the LWR Spent Fuel Assemblies," *Journal of Nuclear Science and Technology*, vol. 33, no. 11, pp. 821–828, Nov. 1996.

[19] D.-G. Lee, J.-H. Park, Y.-H. Lee, C.-Y. Baeg, and H.-J. Kim, "NATURAL CONVECTION HEAT TRANSFER CHARACTERISTICS IN A CANISTER WITH HORIZONTAL INSTALLATION OF DUAL PURPOSE CASK FOR SPENT NUCLEAR FUEL," *Nuclear Engineering and Technology*, vol. 45, no. 7, pp. 969–978, Dec. 2013.

[20] J. C. Lee, W. S. Choi, K. S. Bang, K. S. Seo, and S. Y. Yoo, "Thermal-fluid flow analysis and demonstration test of a spent fuel storage system," *Nuclear Engineering and Design*, vol. 239, no. 3, pp. 551–558, Mar. 2009.
[21] Y.-S. Tseng, J.-R. Wang, F. P. Tsai, Y.-H. Cheng, and C. Shih, "Thermal design investigation of a new tube-type dry-storage system through CFD simulations," *Annals of Nuclear Energy*, vol. 38, no. 5, pp. 1088–1097, May 2011.
[22] J. Creer, M. McKinnon, and J. Tanner, "The TN-24P PWR spent fuel storage cask: testing and analyses," 1987.
[23] S. H. Yoo, H. C. No, H. M. Kim, and E. H. Lee, "Full-scope simulation of a dry storage cask using computational fluid dynamics," *Nuclear Engineering and Design*, vol. 240, no. 12, pp. 4111–4122, Dec. 2010.
[24] R. Brewster and E. Baglietto, "CFD analyses of the TN-24p PWR spent fuel storage cask," *ASME*, 2012.
[25] J. Li and Y. Y. Lui, "Thermal modeling of a vertical dry storage cask for used nuclear fuel | Elsevier Enhanced Reader." [Online]. Available: https://reader.elsevier.com/reader/sd/pii/S0029549316000182?token=1E161497690C268AB1D5A5289AFF48DBB48E1D786A8A6031B8FBE466838EA96578F1A871382EE78D63573BEA574BC973. [Accessed: 07-Oct-2019].
[26] T. L. Bergman, A. S. Lavine, and F. P. Incropera, *Fundamentals of Heat and Mass Transfer, 7th Edition*. John Wiley & Sons, Incorporated, 2011.
[27] A. Khabari, "Natural and Forced Convective Heat Transfer Analysis of Nanostructured Surface," *Proceedings of the World Congress on Engineering*, vol. I, pp. 317–319, Jul. 2014.
[28] "Natural Convective Heat Transfer from a Heated Slender Vertical Tube in a Cylindrical Tank," p. 13, 2015.
[29] B. J. Ade and I. C. Gauld, "Decay Heat Calculations for PWR and BWR Assemblies Fueled with Uranium and Plutonium Mixed Oxide Fuel using SCALE," ORNL/TM-2011/290, 1028163, Oct. 2011.
[30] "NRC: 10 CFR 50.46 Acceptance criteria for emergency core cooling systems for light-water nuclear power reactors." [Online]. Available: https://www.nrc.gov/reading-rm/doc-collections/cfr/part050/part050-0046.html. [Accessed: 17-Dec-2019].